

Realistic time-scale fully atomistic simulations of surface nucleation of dislocations in pristine nanopillars

Pratyush Tiwary^{a,*}, Axel van de Walle^b

^a*Department of Applied Physics and Materials Science, California Institute of Technology, Pasadena, CA 91125, United States*

^b*School of Engineering, Brown University, Providence, Rhode Island, Pasadena, RI 02912, United States*

Abstract

We use our recently proposed accelerated dynamics algorithm (Tiwary and van de Walle, 2011) to calculate temperature and stress dependence of activation free energy for surface nucleation of dislocations in pristine Gold nanopillars under realistic loads. While maintaining fully atomistic resolution, we achieve the fraction of a second time-scale regime. We find that the activation free energy depends significantly and non-linearly on the driving force (stress or strain) and temperature, leading to very high activation entropies. We also perform compression tests on Gold nanopillars for strain rates varying between 7 orders of magnitudes, reaching as low as $10^3/s$. Our calculations bring out the perils of high strain-rate Molecular Dynamics calculations: we find that while the failure mechanism for $\langle 001 \rangle$ compression of Gold nanopillars remains the same across the entire strain-rate range, the elastic limit (defined as stress for nucleation of the first dislocation) depends significantly on the strain-rate. We also propose a new methodology that overcomes some of the limits in our original accelerated dynamics scheme (and accelerated dynamics methods in general). We lay out our methods in sufficient details so as to be used for understanding and predicting deformation mechanism under realistic driving forces for various problems.

Keywords: Dislocations, Molecular Dynamics, Atomistic simulation, Nucleation, Activation Energy, Accelerated Dynamics, Nanomechanics

*Corresponding author

Email addresses: `pt@caltech.edu` (Pratyush Tiwary), `avdw@brown.edu` (Axel van de Walle)

1. Introduction

Forming a correct picture of dislocation nucleation is central to our understanding of deformation mechanisms at the nano-scale. The initial discoveries by Uchic and subsequent work by various groups (Uchic et al., 2004; Wu et al., 2005; Greer et al., 2005, 2009; Volkert and Lilleodden, 2006; Shan et al., 2007; Jennings et al., 2010; Li et al., 2010; Jennings et al., 2011) have now established that there is a marked increase of yield strength as the specimen size decreases, with significant strain-rate dependence as well. These observations have generally been attributed to the scarcity of dislocation sources (such as Frank-Read sources) in nanosized samples, and having to nucleate dislocations in a perfect crystal (perfect apart from presence of surfaces) (Greer and Nix, 2006; Nix et al., 2007; Zhu and Li, 2010; Weinberger and Cai, 2012). As such there have been numerous attempts to link simulations of dislocation nucleation processes to experimentally observed mechanical behavior - in fact a lot of crucial insight has come from simulations (Bulatov et al., 1997; Marian et al., 1997; Moriarty et al., 2002; Li et al., 2002; Abraham et al., 2002; Cao et al., 2007; Zhu et al., 2008; Ryu et al., 2011). Nanoindentation experiments (Landman et al., 1990; Schuh et al., 2005; Schuh, 2006), Scanning Electron Microscopy combined with Nanoindentation (Jang and Greer, 2010), and High Resolution Transmission Electron Microscopy (HRTEM)(Zheng et al., 2010) are now sufficiently advanced for one to hope for a direct match between simulations and experiments (Van Vliet et al., 2003; Zhao et al., 2003; Greer et al., 2008; Zheng et al., 2010).

There are three broad classes of techniques for such simulations, often used in conjunction with each other and along with approaches such as Transition State Theory: classical Molecular Dynamics, continuum based methods and *ab initio* techniques. *Ab initio* simulations, though they often provide insight into mechanical behavior (Arias and Joannopoulos, 1994; Sitch et al., 1995; Woodward and Rao, 2002; Woodward et al., 2008; Carter, 2008), are still restricted to very small sizes, less than a hundred atoms typically (although there are several promising attempts at bridging this length-scale gap for *ab initio* calculations (Fago et al., 2004; Gavini et al., 2007a,b; Trinkle, 2008)). The achievable time-scales are also typically restricted to less than a few picoseconds. Continuum based methods are another elegant option

capable of dealing with a variety of length and time scales, though they suffer from not providing atomic scale resolution and assuming elastic behavior even at dislocation cores (Hirth and Lothe, 1982; Cai et al., 2006; Weinberger et al., 2012). Classical Molecular Dynamics (MD) can be helpful in gaining quantitative insight into mechanical behavior at various length scales (nanometers to microns or larger) (Zhou et al., 1998; Chang et al., 2002; Diao et al., 2006; Park et al., 2006; Rabkin et al., 2007; Li et al., 2010). MD does not assume much apart from the form of interatomic interaction, which is typically developed by fitting to first principles or experimental data. The availability of quality interatomic force-fields (Foiles et al., 1986; Justo et al., 1998; Grochola et al., 2005; Rabkin et al., 2007) and increase in computer power has led to a tremendous increase in the popularity of MD over the last decade.

However, most of the interesting dynamics happens only as the system moves from one energy basin to another through infrequent, rare events. Most of the simulation time gets spent with the system staying stuck in some energy basin (Laio and Parrinello, 2002). This behavior, combined with the femtosecond timestep required for total energy conservation, gives rise to a major limitation of MD: the time-scale problem (Voter et al., 2002; Kushima et al., 2011; Li et al., 2011). Even with the advent of powerful supercomputers, MD simulations are unable to reach more than a few nanoseconds of time if the system size is more than a few hundred atoms. Thus while laboratory strain-rates are typically in the range 10^{-5} - 10^3 /sec, with corresponding activation free energies being around $30k_B T$, MD is unable to go slower than 10^7 /sec strain-rate, corresponding to free energies of around $5k_B T$ or lower (Zhu et al., 2008; Hara and Li, 2010; Ryu et al., 2011; Tiwary and van de Walle, 2011). One approach to get around this shortcoming is to perform 0 temperature Nudged Elastic Band calculation (Henkelman et al., 2000) of the activation free energy and how it varies with applied stress, and then either assume it to be temperature independent, or assume a phenomenological model for its variation with temperature (such as multiplying it with an empirical temperature dependent scaling factor) (Weinberger et al., 2012). These approaches can sometimes work well, but as shown by Hara and Li (2010); Ryu et al. (2011) and in this current work, can sometimes lead to significant inaccuracies in the predictions, such as errors of several orders of magnitude in the nucleation rate, or even qualitatively incorrect phase transitions (Warner and Curtin, 2009).

We recently proposed a hybrid method that combines the strengths of MD and Monte Carlo (MC) simulations in an easily implementable manner and enables one to reach milliseconds and longer times for several thousands of atoms (Tiwary and van de Walle, 2011). The method was recently applied to vacancy diffusion in BCC Fe at low temperature as well as calculation of stress-strain behavior for Au nanowire compression. In both cases it was found to predict correct dynamics, with excellent scaling in computational efficiency with system size. The algorithm was particularly designed to be used on massively parallel computer systems. The main advantages of this new method over existing accelerated MD techniques (see, for e.g., Voter (1997); Voter et al. (2002); Miron and Fichthorn (2003); Lu et al. (2010)) are that (i) it provides a statistically more accurate “real” time scale (which is important when determining the actual strain rate in a simulation and time-dependent forces in general), (ii) it does not rely on transition state theory (which is important when the object of interest is the entropy of activation or migration), (iii) it does not require the specification of the degrees of freedom of interest (which is crucial when the mechanisms are complex and involve the movement of many atoms) and (iv) the efficiency of estimating the “real” time scale (as in (i)) improves linearly with number of computer processors employed for the calculation.

It has remained an unsolved problem so far to design and perform fully atomistic simulations that could provide a picture of temperature dependent activation free energies of dislocation nucleation from surfaces at realistic loads and loading rates. Such a picture is key to linking experimental results with simulation predictions (Warner and Curtin, 2009; Ryu et al., 2011; Weinberger et al., 2012). The critical nucleus for surface nucleation can be as small as a few atomic planes, thus questioning the applicability of continuum methods. As for classical MD, the time-scale achievable is several orders of magnitude smaller than experiments, thus limiting MD simulations to regimes of extremely high nucleation rates. With our recently proposed hybrid MC-MD method that allows us to achieve extended time-scales while still maintaining atomistic resolution, we are able to study the temperature dependence of activation parameters for surface nucleation of dislocations in pristine nanowires and obtain several significant results in an activation regime actually achievable in laboratory experiments. The specific problem we consider pertains to several nano-indentation experiments

where it was found that even if the applied stress on a sample is in the elastic regime, yielding could occur after a certain statistically distributed waiting time (Zuo et al., 2005; Zuo and Ngan, 2006; Mason et al., 2006). We perform fully atomistic simulations of this time-dependent incipient plasticity behavior in Gold nanowires, reaching hundreds of milliseconds time-scales for several thousand atoms. After collecting statistics for various temperatures and applied stresses, we then derive the full picture of stress and temperature dependence of the activation free energy.

In Section 2, we provide a brief summary of our hybrid method in order to facilitate further discussion and keep this paper self-contained. For a more detailed explanation of terms we refer the reader to Tiwary and van de Walle (2011). In the current paper, we also propose a new adiabatic switching technique that significantly reduces the number of input parameters in our hybrid MC-MD approach and eliminates some of the fundamental limitations of our earlier implementation (that were shared by related algorithms (Voter, 1997)). The algorithms employed here make it possible to achieve linear scaling in efficiency of estimating the accelerated time as the number of parallel processors employed is increased. We describe our algorithm and its implementation in sufficient detail for researchers to be able to use it for their problem of interest, and hope that it will be found helpful for modeling a variety of mechanical behavior problems.

2. Details of calculations

2.1. Choice of interatomic potential

There are several good potentials available for modeling mechanical behavior of Gold (Foiles et al., 1986; Cai and Ye, 1996; Park and Zimmerman, 2005; Grochola et al., 2005). The embedded atom method potential by Grochola et al. (2005) gives very realistic values for the surface energy and the stacking fault energy (Rabkin et al., 2007): the stacking fault energy from the potential by Grochola et al. (2005) is $42 \text{ mJ}/m^2$ while the experimental value for it is in the range $32\text{-}46 \text{ mJ}/m^2$. Since the current paper deals with nucleation of dislocations from surfaces, we choose the Grochola potential. This potential was also used and found to perform very well in a recently published joint computational and experimental work studying dislocation behavior in sub-10nm Gold nanowires (Zheng et al., 2010). Rabkin et al.

(2007) provide a critical comparison of this potential with other available potentials for various physical properties relevant to the current work.

2.2. *Hybrid stochastic and deterministic technique for achieving realistic time-scales*

2.2.1. *Summary of ideas*

We recently proposed using a combination of MD and MC techniques for achieving long time scales (Tiwary and van de Walle, 2011). Our approach is built upon minimizing the MD time spent in low-lying energy basins, and instead using 2 kinds of MC simulations. One (a) seeks to properly thermalize the system between infrequent events, thereby minimizing artificial correlations, and the other (b) provides independent control over the accuracy of the time-scale correction. When the potential energy $V(x)$ of the system (where x is a point in the 3-N dimensional configuration space for a system with N particles) is above a certain V_0 , the system evolves as per regular MD (see Fig. 1 in Tiwary and van de Walle (2011)). This high energy region of the phase space is the one containing the interesting but infrequent events. When the system potential energy goes below V_0 , we allow MD to continue until the system has lost memory of how it entered this well (defined as all points x such that $V(x) \leq V_0$). We found that a simple and appropriate criterion to check for this memory loss is when the energy reaches the system's mean energy at that temperature (although other choices are possible, such as letting MD continue for a sufficiently long, user-specified, time or for a random length of time drawn from a user-specified exponential distribution). During this thermalization time, the system may escape the well, in which case the system simply keeps evolving via MD. Most likely, however, the system will not escape the well during that time. When this happens, we stop MD and launch the first MC simulation (called MC *a*). MC *a* runs with a perfectly uniform potential inside the well, rejecting all moves that lead to $V(x) > V_0$. The purpose of MC simulation *a* is to generate a new, properly thermalized, starting point for MD. MD resumes with positions drawn from the last MC *a* step that visited the boundary of the well (defined rigorously in Eq.(2)), and velocities drawn from a Maxwell-Boltzmann distribution in the half space pointing outward of the well. V_0 can be picked high or low depending on the speed-up relative to MD we seek for a particular application. The method is formally correct for any choice of V_0 ; a higher choice of V_0 limits our ability to monitor the detailed dynamics of some events.

We also need to estimate the expected value of the time the system would have spent in the energy well \mathbf{W} , which can be calculated as the reciprocal of the flux exiting the well:

$$t_{\mathbf{W}} = \lim_{w \rightarrow 0} \left(\left\langle \frac{\bar{v}}{w} \mathbf{1}(x \in \mathbf{S}_w) \right\rangle \right)^{-1} \quad (1)$$

where the average $\langle \dots \rangle$ is taken over x drawn from the well \mathbf{W} with a probability density proportional to $e^{-V(x)/(k_B T)}$. k_B is Boltzmann's constant, T is the temperature and the following definitions hold: $\mathbf{1}(A)$ equals 1 if the event A is true and 0 otherwise, \mathbf{S}_w is a shell of width w at the boundary of the well \mathbf{W} , which can be defined in the limit of small w as

$$\mathbf{S}_w = \{x : |V(x) - V_0| \leq w|\nabla V(x)|/2\} \quad (2)$$

\bar{v} denotes the mean projection of a Maxwell-Boltzmann-distributed velocity along the unit vector u parallel to $\nabla V(x)$, conditional on $v \cdot u > 0$. When all atoms have the same mass m , $\bar{v} = \sqrt{k_B T / 2\pi m}$ (a general expression can be found in Tiwary and van de Walle (2011)).

Since Eq.(1) involves an average, it can be approximated using MC simulations. We make use of the system's ergodicity, replacing the time average (that would require us to wait for long times for it to converge) by an ensemble average. Thus in parallel to MC a , we launch several instances (as many as number of available processors) of a second kind of MC simulation, called MC b , to estimate the time-scale correction. A most straightforward implementation of this still won't be as effective in estimating the average in Eq.(1) because the shell \mathbf{S}_w would be visited very rarely. Thus, to improve the efficiency in estimating Eq.(1), we proposed in Tiwary and van de Walle (2011) using a biased potential $V^*(x)$, which is the same as the true potential $V(x)$ in the high energy regions but lifted up in the energy basins (Voter, 1997; Voter et al., 2002). Several lifting (or biasing) schemes are available for use in this (Voter et al., 2002). A simple importance sampling expression (as detailed in Tiwary and van de Walle (2011)) can thus give us the following time-correction:

$$t_{\mathbf{W}} = \lim_{w \rightarrow 0} \frac{\langle e^{-\beta(V(x) - V^*(x))} \rangle^*}{\langle \frac{\bar{v}}{w} e^{-\beta(V(x) - V^*(x))} \mathbf{1}(x \in \mathbf{S}_w) \rangle^*} \quad (3)$$

where $\langle \dots \rangle^*$ denote expectations taken under a density proportional to $e^{-\beta V^*(x)}$, in which β is $1/(k_B T)$. This approach works well, but there is a

fundamental trade-off that limits its usefulness. Lifting the biased potential more and more leads to the energy shell \mathbf{S}_w being visited more frequently and should lead to greater computational efficiency in estimating Eq.(1). However a compensating effect leads to a decrease in efficiency beyond a certain amount of biasing. This is because increased biasing of the potential leads to noisier statistical averaging of the time in Eqs.(1) and (3) - as biasing increases, $(V(x) - V^*(x))$ becomes a large number causing $e^{-\beta(V(x)-V^*(x))}$ to dramatically increase. This point has been discussed in detail in Miron and Fichthorn (2003); Hara and Li (2010); Tiwary and van de Walle (2011). Note that $t_{\mathbf{W}}$ need not be computed for every well the system visits. The overall time scaling only depends on the average escape time, which may be well estimated by a converged average of $t_{\mathbf{W}}$ over a number of wells, though not necessarily *all* wells, but instead over a randomly chosen sampling of all the wells.

2.2.2. Adiabatic switching technique

We now propose a technique that bears some resemblance to adiabatic switching methods (see, e.g. (Tuckerman, 2010)) that helps us deal with the trade-off discussed above, and also eliminates the need for picking a particular biasing scheme. The motivation here is to avoid the statistical noise in Eq.(3) that arises as the biased potential $V^*(x)$ becomes increasingly different from the true potential $V(x)$. To avoid this noise in sampling, the system is continuously, *adiabatically* switched from $V(x)$ (the true potential) to V_0 (a flat potential within the well, identical to the potential used in MC simulation a for thermalization). We now formally derive the method.

Let $\hat{V}(x, \alpha)$ smoothly interpolate between $\hat{V}(x, 0) \equiv V(x)$ and $\hat{V}(x, 1) \equiv V_0$. Then we can express the ensemble average in Eq.(1) as below (working in terms of $rate = 1/time$):

$$\begin{aligned}
 rate &= \lim_{w \rightarrow 0} \frac{\int \frac{\bar{v}}{w} \mathbf{1}(x \in S_w) e^{-\beta \hat{V}(x, 0)} dx}{\int e^{-\beta \hat{V}(x, 0)} dx} \\
 &= \lim_{w \rightarrow 0} \frac{\int \frac{\bar{v}}{w} \mathbf{1}(x \in S_w) e^{-\beta(\hat{V}(x, 0) - \hat{V}(x, 1))} e^{-\beta \hat{V}(x, 1)} dx}{\int e^{-\beta \hat{V}(x, 1)} dx} \left(\frac{\int e^{-\beta \hat{V}(x, 1)} dx}{\int e^{-\beta \hat{V}(x, 0)} dx} \right) \\
 &\equiv \lim_{w \rightarrow 0} \left\langle \frac{\bar{v} \mathbf{1}(x \in S_w)}{w} e^{-\beta(\hat{V}(x, 0) - \hat{V}(x, 1))} \right\rangle_1 R \tag{4}
 \end{aligned}$$

where dx denotes a differential volume in 3-N dimensional configuration space for N particles, the integration being performed over entire configuration space within the well \mathbf{W} and the expected value $\langle \dots \rangle_\alpha$ in Eq.(4) is defined by

$$\langle \dots \rangle_\alpha = \frac{\int (\dots) e^{-\beta \hat{V}(x,\alpha)} dx}{\int e^{-\beta \hat{V}(x,\alpha)} dx} \quad (5)$$

Below we define the term R in Eq.(4) and re-express it in a computationally tractable form:

$$\begin{aligned} R &= \frac{\int e^{-\beta \hat{V}(x,1)} dx}{\int e^{-\beta \hat{V}(x,0)} dx} \\ &= \exp \left(\ln \int e^{-\beta \hat{V}(x,1)} dx - \ln \int e^{-\beta \hat{V}(x,0)} dx \right) \\ &= \exp \left(\int_0^1 \left(\frac{\partial}{\partial \alpha} \ln \int e^{-\beta \hat{V}(x,\alpha)} dx \right) d\alpha \right) \\ &= \exp \left(-\beta \int_0^1 \frac{\int \frac{\partial \hat{V}(x,\alpha)}{\partial \alpha} e^{-\beta \hat{V}(x,\alpha)} dx}{\int e^{-\beta \hat{V}(x,\alpha)} dx} d\alpha \right) \\ &= \exp \left(-\beta \int_0^1 \left\langle \frac{\partial \hat{V}(x,\alpha)}{\partial \alpha} \right\rangle_\alpha d\alpha \right) \end{aligned} \quad (6)$$

With this we can now write the rate in Eq.(4) as

$$rate = \lim_{w \rightarrow 0} \bar{v} \left\langle \frac{1(x \in S_w)}{w} e^{-\beta(\hat{V}(x,0) - \hat{V}(x,1))} \right\rangle_1 \exp \left(-\beta \int_0^1 \left\langle \frac{\partial \hat{V}(x,\alpha)}{\partial \alpha} \right\rangle_\alpha d\alpha \right) \quad (7)$$

We now make a few observations regarding the above expression. It involves 3 independent parts. The first is \bar{v} , which we already know as $\sqrt{k_B T / 2\pi m}$ for identical atoms. We could keep \bar{v} inside the ensemble average to cover the general case of unequal masses in which \bar{v} may depend on x . The second part in Eq.(7) is $\lim_{w \rightarrow 0} \left\langle \frac{1(x \in S_w)}{w} e^{-\beta(\hat{V}(x,0) - \hat{V}(x,1))} \right\rangle_1$. This is non-0 only when $x \in S_w$, and whenever it is non-0, the difference $\hat{V}(x,0) - \hat{V}(x,1)$ is a very small number (see Eq.(2)). Since this average is calculated with a flat potential $\hat{V}(x,1)$, the boundary $x \in S_w$ is visited frequently, and thus the second term in Eq.(7) can be evaluated very quickly - in a few MC passes

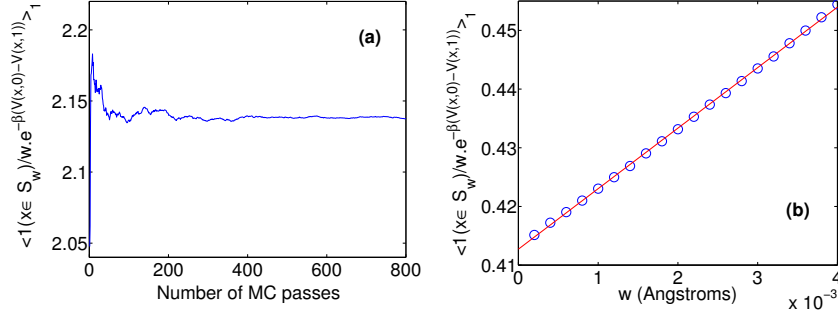


Figure 1: (a) The 2nd part in Eq.(7), i.e. $\left\langle \frac{1(x \in S_w)}{w} e^{-\beta(\hat{V}(x,0) - \hat{V}(x,1))} \right\rangle_1$, can be evaluated in a very small number of MC passes as explained in the text. (b) Calculating $\lim_{w \rightarrow 0} \left\langle \frac{1(x \in S_w)}{w} e^{-\beta(\hat{V}(x,0) - \hat{V}(x,1))} \right\rangle_1$ using linear extrapolation. Calculations are for a Au nanowire with 2016 atoms, 2.5nm in diameter and 7.5nm in height, at 300 K.

as shown in figure 1(a). We calculate $M \equiv \left\langle \frac{1(x \in S_w)}{w} e^{-\beta(\hat{V}(x,0) - \hat{V}(x,1))} \right\rangle_1$ for a few values of w , and simple linear extrapolation gives the desired limit, as shown in figure 1(b). The third part in Eq.(7) is $\exp\left(-\beta \int_0^1 \left\langle \frac{\partial \hat{V}(x, \alpha)}{\partial \alpha} \right\rangle_\alpha d\alpha\right)$. Here, the average $\left\langle \frac{\partial \hat{V}(x, \alpha)}{\partial \alpha} \right\rangle_\alpha$ does not contain any exponentials, and thus no terms that could blow-up and lead to noisy estimates and slow convergence.

We now need to pick up a switching scheme for $\hat{V}(x, \alpha)$, i.e. an interpolation scheme between $\hat{V}(x, 0)$ and $\hat{V}(x, 1)$. We picked the simplest scheme - a linear switching model - and found it to work very well:

$$\hat{V}(x, \alpha) = (1 - \alpha)V(x) + \alpha V_0 \quad (8)$$

With this, Eq.(7) for the rate of escaping energy basins bounded by $V(x) < V_0$ becomes

$$rate = \lim_{w \rightarrow 0} \bar{v} \left\langle \frac{1(x \in S_w)}{w} e^{-\beta(\hat{V}(x,0) - \hat{V}(x,1))} \right\rangle_1 \exp\left(\beta \int_0^1 \langle V(x) - V_0 \rangle_\alpha d\alpha\right) \quad (9)$$

Thus to summarize till this point, to calculate Eq.(9), we first do a quick MC simulation using a flat potential to get $\lim_{w \rightarrow 0} \left\langle \frac{1(x \in S_w)}{w} e^{-\beta(\hat{V}(x,0) - \hat{V}(x,1))} \right\rangle_1$, as shown in figure 1. We then vary α adiabatically during the simulation, going from $\alpha = 0$ to $\alpha = 1$. We perform a series of MC simulations, with the Hamiltonian of the system evolving as per Eq.(8) as the simulation time

progresses. A typical evaluation of Eq.(9) done as per this scheme is shown in figure 2, where we show the change in the following two as a function of α : (a) $\left(-\beta \int_0^1 \left\langle \frac{\partial \hat{V}(x,\alpha)}{\partial \alpha} \right\rangle_\alpha d\alpha\right)$, related to the 3rd part in Eq.(9), and (b) the expected value of the time spent in the energy well \mathbf{W} .

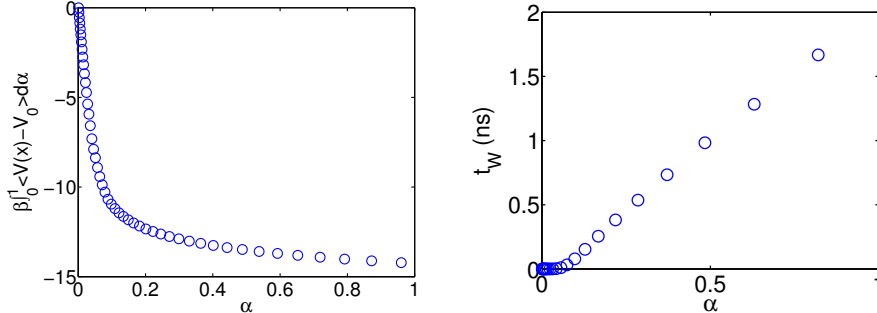


Figure 2: (a) Change in $\left(-\beta \int_0^1 \left\langle \frac{\partial \hat{V}(x,\alpha)}{\partial \alpha} \right\rangle_\alpha d\alpha\right)$ as a function of α as the simulation progresses (see Eq.(7)). (b) Expected value of the time spent in the energy well \mathbf{W} . Calculations are for a Au nanowire with 2016 atoms, 2.5nm in diameter and 7.5nm in height, at 300 K.

It may be useful to emphasize one point: The reason we do not immediately start MC as soon as $V(x)$ falls below V_0 is because the rate expression (Equation (1)) is only valid conditional on the system being initialized at a Boltzman-distributed random position within the well. If we start MC at the boundary of the well, this assumption is violated. Although it may seem that, by running MD within the well for some time before calculating the escape rate, we slightly overestimate the time spent in the well, this is not the case. The distribution of escape time from the well is independent of the time already spent in the well (since it follows an exponential distribution). Another way to see that there is no time over-counting is to observe that, during this MD trajectory in the well, there is also a small probability that the system escapes the well, so we are not artificially constraining the system to remain in the well for a longer time. The above scheme is a new, yet formally correct, way to deal with so-called re-crossing events that typically affect the accuracy of transition-theory based estimates of escape times (Voter et al., 2002; Lu et al., 2010).

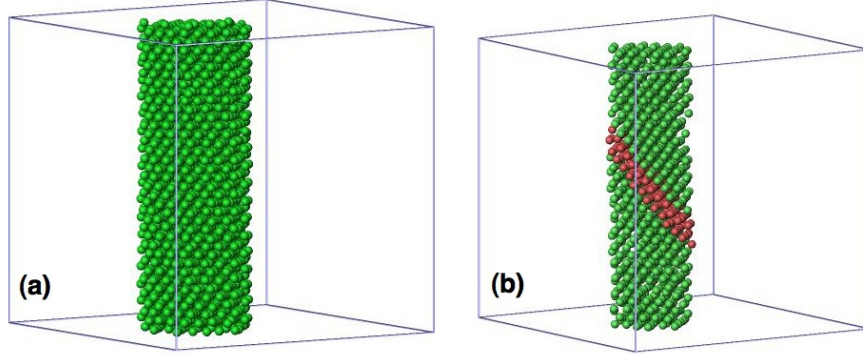


Figure 3: Perspective view of the nanopillar (a) before application of strain and (b) after application of strain when partial dislocation has nucleated. Coloring is as per Common Neighbor Analysis(Honeycutt and Andersen, 1987), where green denotes FCC, red denotes HCP. In (b), the surface atoms (identified as atoms that are neither FCC nor HCP) have been removed to bring the slip plane into clarity. Visualization was carried using the package OVITO(Stukowski, 2010).

2.3. Simulation set-up and compression testing

We first report the stress-strain plots for $\langle 001 \rangle$ compression of pristine cylindrical Au nanowires. The cylinder was initially carved out from perfect FCC lattice and before compression, it was 2.5nm in diameter and 7.5nm in height, comprising 2016 atoms (see figure 3) with periodic boundary conditions imposed along all three directions. The cylinder axis z is also the compression axis $\langle 001 \rangle$. Thus all sites along the length of the wire are now equivalent sites for nucleation. For the other two directions, we do not strictly need periodic boundary conditions, but we nevertheless apply it for computational ease. The dimensions of the supercell in the x and y directions are both around 75\AA , which is much larger than the range of the EAM potential employed (5.5\AA)(Grochola et al., 2005). As such there is no artifact from the pillar interacting with its images in these two directions. The cylinder was first equilibrated for 500 ps before beginning the compression, which was carried out by uniformly re-scaling the z -coordinates of all atoms. The atomic virial stress was used to obtain the Cauchy stress(Rabkin et al., 2007). The stress at zero nominal strain is non-zero and tensile, and arises from the surface stress (see Rabkin et al. (2007); Weinberger et al. (2012) for a more detailed explanation). We adjust for this, and as such figure 4 provides the

stress span, i.e. the stress at a strain ϵ relative to the stress at 0 strain. We present the resulting stress(σ) versus nominal strain(ϵ) plots for 2 different strain rates $\dot{\epsilon}$: 5×10^7 /sec, a strain rate value used in current day state-of-the-art MD simulations, and 10^3 /sec. To the best of our knowledge, the latter is a strain rate several orders of magnitude slower than any reported calculation for a nanowire, and is a value that can actually be achieved in laboratory experiments on nanowires.

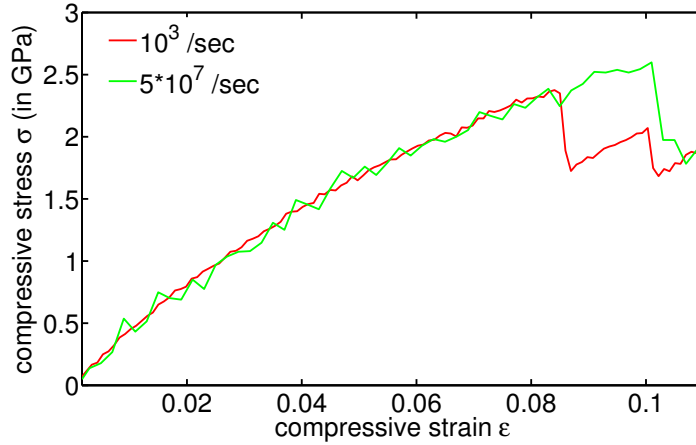


Figure 4: The stress versus nominal strain curve of Au nanowire under $\langle 001 \rangle$ compression (with inverted sign of stress). The data represents stress relative to surface stress at 0 strain as explained in text. The stress-strain plots are shown for two different strain rates. The green line denotes our calculations for a strain rate of 5×10^7 /sec, which is a commonly used strain rate in current-day MD. The red line shows our calculations for a strain rate of 10^3 /sec.

For the strain rate of 5×10^7 /sec, it was sufficient to perform ordinary NVT MD simulations using a time step of 2×10^{-15} sec and a Langevin thermostat with a coupling constant 1×10^{-11} /sec. For the strain rate of 10^3 /sec which can not be achieved through plain MD, we used our hybrid MC-MD algorithm as described in the preceding section and in Tiwary and van de Walle (2011). The time-step and thermostat were same as for the strain rate of 5×10^7 /sec. All the calculations were performed on our in-house parallel MD package. Starting value of V_0 was picked such that it gave a rough $t_{\mathbf{W}}$ of around 1 nanosecond (see table 1). This was a value high enough for our

current application. As the temperature/driving force (stress or strain) decrease, one would pick a higher V_0 that would accordingly lead to a larger $t_{\mathbf{W}}$. During compression as work is being performed on the system, there is a change in the potential energy, and as such the value of V_0 was updated every few thousand MD steps by an amount equaling the change in the mean potential energy over these many MD steps. A sharp drop in the potential energy indicates that a (partial) dislocation nucleation event has occurred in the system (see figure 5). Table 1 provides values of the various parameters used in the compression testing experiment.

For both of these strain rates, the yielding is through slip and not twinning or elastic instabilities: a leading Shockley partial nucleates on a $\{111\}$ slip plane at lower stresses than a trailing partial. This can be seen in figure 3(b) where the leading partial nucleated from the surface and left behind a 2-layer thick HCP region. The trailing and leading partials are in agreement with what one expects by calculating relative Schmid factors: for $\langle 001 \rangle$ compression, $(a/6)[11\bar{2}]$ and $(a/6)[\bar{2}11]$ were found to be the leading and trailing partials corresponding to Schmid factors of 0.47 and 0.24 respectively (Weinberger et al., 2012).

Table 1: Starting value of V_0 and expected value of $t_{\mathbf{W}}$, for unstrained samples at various temperatures. For strained samples, the change in potential energy during the process of straining was calculated, and V_0 was changed by this amount. For the temperatures between 350K to 425 K, ordinary MD was sufficient for the stress range considered in this work and hence the parameters below are only for temperatures till 325 K.

T(K)	V_0 (eV)	$t_{\mathbf{W}}$ (ps)
275	-7275.00	1400
300	-7267.75	1700
325	-7260.25	30

Figure 4 brings out the perils of using unrealistic strain-rate MD calculations as a tool for insight and discovery. We find that though the failure mechanism stays same for both the strain-rates, there is a significant difference in the strain at which slip occurs. At the high strain-rate of 5×10^7 /sec, the wire withstands strain of as high as almost 10% before the first partial dislocation is emitted (corresponding to a stress span of around 2.6 GPa). However at the more realistic strain rate of 10^3 /sec, the partial is emitted

around 8.6% only (corresponding to a stress span of around 2.35 GPa). For both the strain-rates, there is a distribution of the strain at which slip occurs and the values in 3) denote mean values.

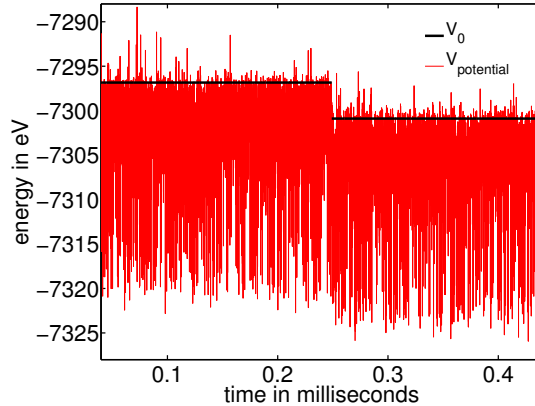


Figure 5: Typical variation of the energy lid V_0 (black line) and potential energy (red line) as a function of time. V_0 is adjusted as per the change in mean potential energy every few thousand MD steps. A sharp drop in the potential energy and accordingly in V_0 indicates that a nucleation event has occurred.

This strong difference is in accordance with the strain-rate sensitivity in true nanowires (i.e. wires less than 100nm in diameter) as predicted by Zhu et al. (2008) and observed in real experiments on small nanowires by Jennings et al. (2011). To understand and motivate this dependence, we look at the rate of nucleation of leading partial dislocation, as given by Eq. (10) below (Zhu et al., 2008):

$$R = N\nu(\epsilon).exp\left(\frac{-F(\epsilon, T)}{k_B T}\right) \quad (10)$$

Here F is the Helmholtz free energy of activation as a function of temperature T and strain ϵ (since our experimental set-up is a constant strain situation), $k_B T$ is the thermal energy, N is the number of equivalent surface nucleation sites and $\nu(\epsilon)$ is an athermal strain-dependent attempt frequency. Eq. (10) thus has two contributions: an athermal part related to the elastic limit (which we defined as stress for nucleation of the first dislocation) of the surface at which nucleation would occur spontaneously without any thermal

contributions, and an activated part that takes into account the role of thermal fluctuations in causing nucleation to happen even below the athermal strain (which is the minimum strain at which nucleation would occur at absolute zero temperature).

2.4. Activation Parameters

2.4.1. Activation Volume

The activation volume Ω is defined as the derivative of the activation free energy with respect to stress, i.e. $\Omega(\sigma, T) \equiv -(\frac{\partial F}{\partial \sigma})_T$. As reported through experimental measurements as well as TST based calculations, the activation volume for surface nucleation remains in a characteristic range of few b^3 (where b is the burgers vector). In comparison, for a typical bulk dislocation source the activation volume is upwards of $100b^3$ and can be as high as $1000b^3$ (Jennings et al., 2011). The activation volume in turn determines whether a process will be strain-rate sensitive or insensitive. This can be reasoned as follows. Assuming a simple case where the activation energy depends linearly on stress (see Zhu et al. (2008) for detailed derivation), one can show that the most probable estimate of the nucleation stress is given by

$$\sigma = \sigma_{athermal} - \frac{k_B T}{\Omega} \ln \frac{k_B T N \nu}{E \dot{\epsilon} \Omega} \quad (11)$$

where E is the Young's modulus and $\sigma_{athermal}$ is the athermal nucleation stress causing instantaneous dislocation nucleation. As can be seen in Eq. (11), a high activation volume (as in the case of bulk dislocation source) masks out the effect of strain-rate. As the activation volume decreases towards values relevant for surface nucleation, the effect of strain rate should become very significant. Figure 4 provides the first direct MD based evidence of this.

2.4.2. Activation Free Energy

We now report detailed calculations of the activation terms in Eq. (10). To do so, we performed the compression testing at a strain-rate of 10^3 /sec at 7 different temperatures from 275 K to 425 K at intervals of 25 K. These compression tests were stopped at various values of the nominal strain from 8% to 8.5% (the athermal strain at 0 Kelvin for nanowire of these dimensions was found to be around 13.5%). The wisdom behind choosing this particular

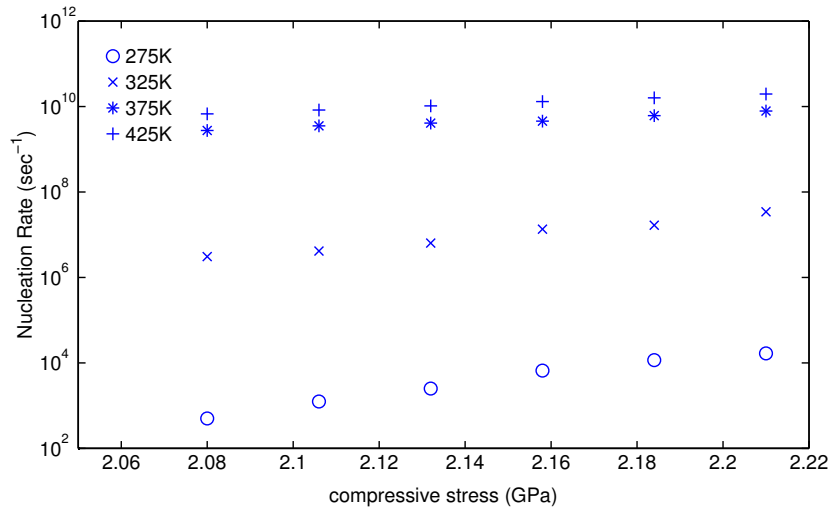


Figure 6: Strain and temperature dependence of the dislocation nucleation rate $R(\epsilon, T)$, converted here to $R(\sigma, T)$ by assuming a linear dependence of stress on strain. Each data point was calculated by averaging over 16 samples. The size of the individual markers corresponds to the 90% confidence interval in the measurement.

range of strain will be clear soon when we provide estimates of the nucleation rate. For each of these strains, the wire is still in the elastic regime. As described in the introduction, we are interested in collecting statistics of the waiting time before nucleation of the first dislocation as the nanowire is held at this strain (Zuo et al., 2005; Zuo and Ngan, 2006). The structures from the compression tests stopped at varying strains served as samples for our waiting time statistics tests.

For each of these structures (corresponding to a combination of imposed strain and temperature), 16 different runs were carried out where the nanowire was held at a particular strain and temperature. Each of the runs was carried out until nucleation of the first dislocation, marked by appearance of a 2-layer thick HCP region, as well as sudden dips in the potential energy and the stress (see figure 5). The average rate of nucleation was then calculated as

$$R(\epsilon, T) = \frac{1}{\tau_{average}} \quad (12)$$

where $\tau_{average}$ is the time for nucleation averaged over the 16 samples.

Figure 6 provides the value for nucleation rate for various strain and temperature combinations. In this figure we have converted strain to stress by assuming a roughly constant Young's Modulus of around 26 GPa as we obtained in figure 4 for $\langle 001 \rangle$ compression of Gold nanowire, in order to facilitate comparison with published literature, even though in figure 4 we see a softening in the tangent modulus as the strain increases. This plot clarifies our choice of imposed strains - with 8% strain (or 2.08 GPa stress), the nucleation rate is already slower than one every few milliseconds at 275K. The other end of 8.5% was picked because as illustrated in figure 4, the wire slips at high temperatures around 8.6%. The lengthiest of these calculations took around a few CPU days. With a slightly more aggressive choice of V_0 , it should be possible to reach the one per second or still slower regime.

For each strain ϵ , we picked a sufficiently high value of reference temperature T_0 such that the rate $R(\epsilon, T_0)$ did not any longer depend on the choice of temperature. We can then make the approximation that $F(\epsilon, T) \gg F(\epsilon, T_0)$, and express Eq.(10) as Eq.(13) below, to factor out the athermal frequency term. Given this approximation, the entropy of activation we calculate subsequently is effectively measured relative to the high temperature limit (since the activation entropy at high temperature could still be nonzero).

$$F(\epsilon, T) \approx -k_B T \ln\left(\frac{R(\epsilon, T)}{R(\epsilon, T_0)}\right) \quad (13)$$

From Eq.(13) we directly calculate the Activation Free Energy $F(\epsilon, T)$ (figure 7). Our values are in the rough benchmark of the 0.3 eV value found in Copper nano-indentation experiments where one expects homogeneous nucleation to be the mechanism at work (Schuh et al., 2005). Figure 7 also provides the only published values of activation free energy at 0 Kelvin temperature for Au nanowires (Weinberger et al., 2012). Weinberger et al. (2012)'s calculations are for a 5nm diameter nanowire (thus 4 times as many atoms as in our nanowire) using a chain of states methodology at 0 Kelvin. A comparison between our and their free energies is thus not really justified due to differing system sizes - this can be understood by looking at Eq. (11). In a larger sample the number of nucleation sites (surface atoms) N is higher. As such the nucleation stress goes down, increasing the probability of nucleation for the same driving force (stress/strain and temperature). This in

turn leads to a lower free energy of activation. Some qualitative differences between these two calculations may will also arise because of difference in interatomic potentials. Even though a direct comparison between Weinberger et al. (2012)’s and our results is not justified due to these reasons, we still provide their results in figure 7) since viewed together our results give a full picture of how the activation free energy varies with stress, temperature and specimen size.

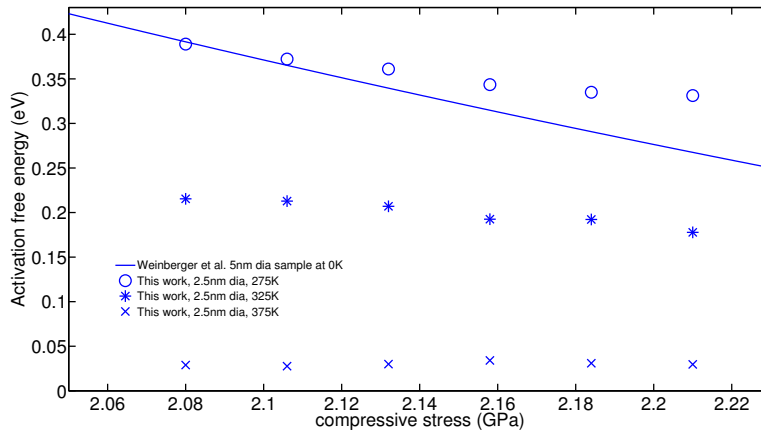


Figure 7: Activation free energy for surface nucleation of dislocations as a function of stress and temperature. Comparisons are made with results from literature for 0 Kelvin activation energy for a wire 8 times bigger (thus with many more possible nucleation sites). The size of the individual markers corresponds to the 90% confidence interval in the measurement.

Our calculations demonstrate how strongly and rather non-linearly the free energy of activation depends on the temperature. It has been a common practice, mostly arising from lack of methods capable of providing high temperature activation energy barriers calculations, to assume the same temperature dependence for activation free energy across temperatures. Many workers have found direct and indirect evidence suggesting this is incorrect for studying deformation in materials. For example, Warner and Curtin (2009) found that in Al, a temperature dependent activation barrier can lead to a transition from twinning to full dislocation emission back to twinning with increasing temperature. We believe our algorithm should now provide

researchers with a tool to calculate such barriers at various temperatures under realistic loading rates for the first time.

2.4.3. Activation Entropy

From the variation of activation free energy with stress and temperature in figure 7, we calculated the stress dependent activation entropy. To obtain this quantity, we do a linear fit between the activation energy and the temperature at each stress value. The entropy is then the slope of this linear fit (with a negative sign), reported in figure 8. Such a calculation has rarely been performed for dislocation nucleation or for other problems - the two instances of such calculations we could find were Hara and Li (2010)'s recent adaptive strain-boost hyperdynamics (ASBHD) where the authors calculate the stress dependent entropy for corner nucleation in Copper nanowires, and Ryu et al. (2011)'s Umbrella Sampling based calculations (in Copper as well). We find that the entropy decreases as the driving force (stress or strain) increases, and is typically in the range $20\text{-}30k_B$. This is roughly in the benchmark of values reported through previous simulations. We avoid making detailed comparisons here between our values and these previously published values, given that we differ in elements (gold versus copper), geometries (circular versus square with sharp cross-sections), size and ensemble (constant stress versus constant strain, see Ryu et al. (2011)).

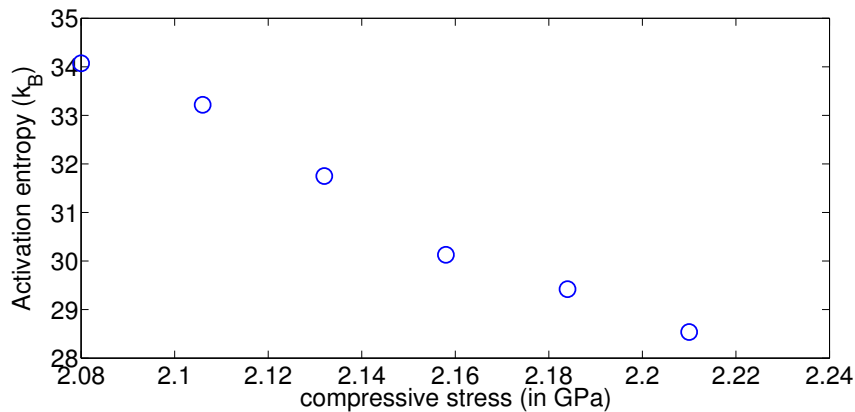


Figure 8: Activation entropy as a function of stress for surface nucleation of dislocations.

3. Discussion

3.1. Key results

Our compressive tests on Au nanopillars show that the mechanism of deformation stays same for strain rates from $10^8/s$ to $10^3/s$, i.e., slip through nucleation of a leading Shockley partial dislocation on a $\{111\}$ slip plane. However, the elastic limit (defined as stress for nucleation of the first dislocation) changes significantly as the strain-rate is changed. This is in qualitative agreement with the strain-rate dependence in nanopillars as observed in experiments (Jennings et al., 2011) and also predicted by the phenomenological models of Zhu et al. (2008). We believe ours is the first fully atomistic calculation reported across 6 orders of magnitudes in the strain-rate and reaching a realistic strain rate of $10^3/s$.

The origin of activation entropy in dislocation nucleation, and related to it the rapid drop of activation free energy with temperature, can be attributed to thermal expansion in the material (Ryu et al., 2011). As the temperature increases the expansion causes atoms to move away from each other making it easier for planes to shear and thus reducing the free energy barrier for nucleation. Our high activation entropy values show that not considering the temperature dependence of the activation energy can lead to nucleation rate being erroneous by as much as 8-12 orders of magnitude. This has been emphasized in the very recent literature by Ryu et al. (2011). We also found that the entropy decreases as the driving force for nucleation (stress or strain) increases, leading to a significant and non-linear dependence of the activation free energy on driving force and temperature. Our method now provides an easy-to-implement way to calculate this dependence under realistic driving forces for any general sample geometry.

3.2. Comparison of our algorithm with other algorithms for extended time-scales

It is also instructive to compare our algorithm with other realistic time-scale algorithms for studying dislocation nucleation. Two algorithms that have been recently used to model temperature-dependence of the dislocation nucleation process include the Umbrella Sampling method (proposed by Ryu et al. (2011)) and the Adaptive Strain Boost Hyperdynamics (ASBHD) method (proposed by Hara and Li (2010)). Both are excellent methods, but

have their respective limitations. The former needs to define an order parameter (or a reaction co-ordinate) for the system, in terms of which the biasing potential is then imposed on a certain sub-set of atoms. Picking such an order parameter might be a non-trivial task in complicated sample geometries and can have its pitfalls (Dickson et al., 2009). Also, while this method is excellent for computing free energy barriers - it does not perform any actual dynamics. ASBHD does away with the need to pick up an order parameter. However the speed-up in ASBHD relative to ordinary MD becomes significant (i.e. 4-5 orders of magnitude or more) only as the temperature of the system falls below 100K or so. The method is a local boost scheme, thus specific atoms are lifted out of the low-lying energy basins, making them preferential sites for nucleation to happen. Such a local boost scheme works well for specific geometries (such as a square nano-rod with sharp corners), but might not be very well suited for studying more homogeneous nucleation as we are considering in the current paper. Since our method does not require the specification of the degrees of freedom of interest (which is crucial when the mechanisms are complex and involve the movement of many atoms), it is well suited for studying homogeneous nucleation.

By providing a time-scale correction independent to the main simulation, our algorithm also provides the ability to implement time-dependent boundary conditions (relevant to a tensile test for e.g.) and in general time-dependent forces. To do this, we can launch a set of adiabatic switching jobs prior to the main simulation, that give a good starting value for the quantity $t_{\mathbf{W}}$ and thus for the boosted time-scale. This is to be contrasted with ASBHD (Hara and Li, 2010) and Hyperdynamics methods in general (Voter, 1997) where time-scale estimates remain noisy and non-converged for long simulation times, especially as one tries to increase the speed-up relative to ordinary MD (Miron and Fichthorn, 2003; Tiwary and van de Walle, 2011).

4. Conclusions

In this paper we have derived and demonstrated a hybrid MC-MD algorithm that can be used to achieve realistic time-scales in fully atomistic simulations of materials while still predicting correct deformation physics. The algorithm is especially designed to be suited for massive parallelization. By using this algorithm, we obtained compression testing stress-strain plots at strain rates several orders of magnitude lower than ever previously re-

ported for MD simulations. We showed that high strain-rates in simulations, which have been common due to lack of methods capable of implementing low strain-rates, can lead to a significant error in the elastic limit (defined earlier) of the material. We also derived the full stress and temperature dependence of the activation free energy for surface nucleation of dislocations in Gold nanowires. The algorithm was described in sufficient detail to be useful to the mechanics community for different applications.

Acknowledgment

We would like to thank Andrew Jennings and Prof. Julia Greer for helpful discussions and comments on the manuscript; Dr. Arthur Voter for helpful discussions regarding the algorithm; and Dr. Seunghwa Ryu for originally suggesting this particular application at a Gordon Research Conference. This research was supported by the US National Science Foundation through XSEDE computational resources provided by NCSA under grant DMR050013N and NSF Condensed Matter and Materials Theory program DMR-0907669.

References

References

- Abraham, F. F., Walkup, R., Gao, H., Duchaineau, M., Diaz De La Rubia, T., Seager, M., 2002. Simulating materials failure by using up to one billion atoms and the world's fastest computer: Work-hardening. *Proceedings of the National Academy of Sciences* 99 (9), 5783–5787.
- Arias, T. A., Joannopoulos, J. D., 1994. *Ab Initio* theory of dislocation interactions: From close-range spontaneous annihilation to the long-range continuum limit. *Phys. Rev. Lett.* 73, 680–683.
- Bulatov, V., Abraham, F. F., Kubin, L., Devincere, B., Yip, S., 1997. Connecting atomistic and mesoscale simulations of crystal plasticity. *Nature* 391, 669 – 672.
- Cai, J., Ye, Y. Y., 1996. Simple analytical embedded-atom-potential model including a long-range force for fcc metals and their alloys. *Phys. Rev. B* 54, 8398–8410.

- Cai, W., Arsenlis, A., Weinberger, C. R., Bulatov, V. V., 2006. A non-singular continuum theory of dislocations. *Journal of the Mechanics and Physics of Solids* 54 (3), 561 – 587.
- Cao, A. J., Wei, Y. G., Mao, S. X., 2007. Deformation mechanisms of face-centered-cubic metal nanowires with twin boundaries. *Applied Physics Letters* 90 (15), 151909.
- Carter, E. A., 2008. Challenges in modeling materials properties without experimental input. *Science* 321 (5890), 800–803.
- Chang, J., Cai, W., Bulatov, V. V., Yip, S., 2002. Molecular dynamics simulations of motion of edge and screw dislocations in a metal. *Computational Materials Science* 23, 111 – 115.
- Diao, J., Gall, K., Dunn, M. L., Zimmerman, J. A., 2006. Atomistic simulations of the yielding of gold nanowires. *Acta Materialia* 54 (3), 643 – 653.
- Dickson, B. M., Makarov, D. E., Henkelman, G., 2009. Pitfalls of choosing an order parameter for rare event calculations. *The Journal of Chemical Physics* 131 (7), 074108.
- Fago, M., Hayes, R. L., Carter, E. A., Ortiz, M., 2004. Density-functional-theory-based local quasicontinuum method: Prediction of dislocation nucleation. *Phys. Rev. B* 70, 100102.
- Foiles, S. M., Baskes, M. I., Daw, M. S., 1986. Embedded-atom-method functions for the fcc metals cu, ag, au, ni, pd, pt, and their alloys. *Phys. Rev. B* 33, 7983–7991.
- Gavini, V., Bhattacharya, K., Ortiz, M., 2007a. Quasi-continuum orbital-free density-functional theory: A route to multi-million atom non-periodic dft calculation. *Journal of the Mechanics and Physics of Solids* 55 (4), 697 – 718.
- Gavini, V., Knap, J., Bhattacharya, K., Ortiz, M., 2007b. Non-periodic finite-element formulation of orbital-free density functional theory. *Journal of the Mechanics and Physics of Solids* 55 (4), 669 – 696.
- Greer, J. R., Jang, D., Kim, J.-Y., Burek, M. J., 2009. Emergence of new mechanical functionality in materials via size reduction. *Advanced Functional Materials* 19 (18), 2880–2886.
- Greer, J. R., Nix, W. D., 2006. Nanoscale gold pillars strengthened through dislocation starvation. *Phys. Rev. B* 73, 245410.

- Greer, J. R., Oliver, W. C., Nix, W. D., 2005. Size dependence of mechanical properties of gold at the micron scale in the absence of strain gradients. *Acta Materialia* 53 (6), 1821 – 1830.
- Greer, J. R., Weinberger, C. R., Cai, W., 2008. Comparing the strength of f.c.c. and b.c.c. sub-micrometer pillars: Compression experiments and dislocation dynamics simulations. *Materials Science and Engineering: A* 493, 21 – 25.
- Grochola, G., Russo, S. P., Snook, I. K., 2005. On fitting a gold embedded atom method potential using the force matching method. *The Journal of Chemical Physics* 123 (20), 204719.
- Hara, S., Li, J., 2010. Adaptive strain-boost hyperdynamics simulations of stress-driven atomic processes. *Phys. Rev. B* 82, 184114.
- Henkelman, G., Uberuaga, B. P., Jonsson, H., 2000. A climbing image nudged elastic band method for finding saddle points and minimum energy paths. *The Journal of Chemical Physics* 113 (22), 9901–9904.
- Hirth, J., Lothe, J., 1982. *Theory of dislocations*, second edition.
- Honeycutt, J. D., Andersen, H. C., 1987. Molecular dynamics study of melting and freezing of small lennard-jones clusters. *The Journal of Physical Chemistry* 91 (19), 4950–4963.
- Jang, D., Greer, J. R., 2010. Transition from a strong-yet-brittle to a stronger-and-ductile state by size reduction of metallic glasses. *Nature Materials* 9 (3), 215 – 219.
- Jennings, A. T., Burek, M. J., Greer, J. R., 2010. Microstructure versus size: Mechanical properties of electroplated single crystalline cu nanopillars. *Phys. Rev. Lett.* 104, 135503.
- Jennings, A. T., Li, J., Greer, J. R., 2011. Emergence of strain-rate sensitivity in cu nanopillars: Transition from dislocation multiplication to dislocation nucleation. *Acta Materialia* 59 (14), 5627 – 5637.
- Justo, J. a. F., Bazant, M. Z., Kaxiras, E., Bulatov, V. V., Yip, S., 1998. Interatomic potential for silicon defects and disordered phases. *Phys. Rev. B* 58, 2539–2550.
- Kushima, A., Eapen, J., Li, J., Yip, S., Zhu, T., 2011. Time scale bridging in atomistic simulation of slow dynamics: viscous relaxation and defect activation.

The European Physical Journal B - Condensed Matter and Complex Systems
82, 271–293.

- Laio, A., Parrinello, M., 2002. Escaping free-energy minima. *Proceedings of the National Academy of Sciences* 99, 12562–12566.
- Landman, U., Luedtke, W. D., Burnham, N. A., Colton, R. J., 1990. Atomistic mechanisms and dynamics of adhesion, nanoindentation, and fracture. *Science* 248 (4954), 454–461.
- Li, J., Sarkar, S., Cox, W. T., Lenosky, T. J., Bitzek, E., Wang, Y., Aug 2011. Diffusive molecular dynamics and its application to nanoindentation and sintering. *Phys. Rev. B* 84, 054103.
- Li, J., Van Vliet, Krystyn, J., Zhu, T., Yip, S., Suresh, S., 2002. Atomistic mechanisms governing elastic limit and incipient plasticity in crystals. *Nature* 418, 307.
- Li, X., Wei, Y., Lu, L., Lu, K., Gao, H., 2010. Dislocation nucleation governed softening and maximum strength in nanotwinned metals. *Nature* 464, 877.
- Lu, C.-Y., Makarov, D. E., Henkelman, G., 2010. Communication: kappa-dynamics—an exact method for accelerating rare event classical molecular dynamics. *The Journal of Chemical Physics* 133 (20), 201101.
- Marian, J., Cai, W., Bulatov, V. V., 1997. Dynamic transitions from smooth to rough to twinning in dislocation motion. *Nature* 3, 158 – 163.
- Mason, J. K., Lund, A. C., Schuh, C. A., 2006. Determining the activation energy and volume for the onset of plasticity during nanoindentation. *Phys. Rev. B* 73, 054102.
- Miron, R. A., Fichthorn, K. A., 2003. Accelerated molecular dynamics with the bond-boost method. *Journal of Chemical Physics* 119, 6210.
- Moriarty, J., Vitek, V., Bulatov, V., Yip, S., 2002. Atomistic simulations of dislocations and defects. *Journal of Computer-Aided Materials Design* 9, 99–132.
- Nix, W. D., Greer, J. R., Feng, G., Lilleodden, E. T., 2007. Deformation at the nanometer and micrometer length scales: Effects of strain gradients and dislocation starvation. *Thin Solid Films* 515 (6), 3152 – 3157.

- Park, H. S., Gall, K., Zimmerman, J. A., 2006. Deformation of fcc nanowires by twinning and slip. *Journal of the Mechanics and Physics of Solids* 54 (9), 1862 – 1881.
- Park, H. S., Zimmerman, J. A., Aug 2005. Modeling inelasticity and failure in gold nanowires. *Phys. Rev. B* 72, 054106.
- Rabkin, E., Nam, H.-S., Srolovitz, D., 2007. Atomistic simulation of the deformation of gold nanopillars. *Acta Materialia* 55 (6), 2085 – 2099.
- Ryu, S., Kang, K., Cai, W., 2011. Entropic effect on the rate of dislocation nucleation. *Proceedings of the National Academy of Sciences* 108, 5174.
- Schuh, C. A., 2006. Nanoindentation studies of materials. *Materials Today* 9 (5), 32 – 40.
- Schuh, C. A., Mason, J. K., Lund, A. C., 2005. Quantitative insight into dislocation nucleation from high-temperature nanoindentation experiments. *Nature Materials* 4, 617.
- Shan, Z. W., Mishra, R. K., Syed Asif, S. A., Warren, O. L., Minor, A. M., 2007. Mechanical annealing and source-limited deformation in submicrometre-diameter ni crystals. *Nature materials* 7, 115–119.
- Sitch, P. K., Jones, R., Öberg, S., Heggie, M. I., 1995. *Ab initio* investigation of the dislocation structure and activation energy for dislocation motion in silicon carbide. *Phys. Rev. B* 52, 4951–4955.
- Stukowski, A., 2010. Visualization and analysis of atomistic simulation data with ovito the open visualization tool. *Modelling and Simulation in Materials Science and Engineering* 18, 015012.
- Tiwary, P., van de Walle, A., 2011. Hybrid deterministic and stochastic approach for efficient atomistic simulations at long time scales. *Phys. Rev. B* 84, 100301.
- Trinkle, D. R., 2008. Lattice green function for extended defect calculations: Computation and error estimation with long-range forces. *Phys. Rev. B* 78, 014110.
- Tuckerman, M., 2010. *Statistical mechanics: theory and simulation*.
- Uchic, M. D., Dimiduk, D. M., Florando, J. N., Nix, W. D., 2004. Sample dimensions influence strength and crystal plasticity. *Science* 305 (5686), 986–989.

- Van Vliet, K. J., Li, J., Zhu, T., Yip, S., Suresh, S., 2003. Quantifying the early stages of plasticity through nanoscale experiments and simulations. *Phys. Rev. B* 67, 104105.
- Volkert, C. A., Lilleodden, E. T., 2006. Size effects in the deformation of sub-micron columns. *Philosophical Magazine* 86 (33-35), 5567–5579.
- Voter, A. F., 1997. Hyperdynamics: Accelerated molecular dynamics of infrequent events. *Phys. Rev. Lett.* 78, 3908–3911.
- Voter, A. F., Montalenti, F., Germann, T. C., 2002. Extending the time scale in atomistic simulation of materials. *Annual Review of Materials Research* 32 (1), 321–346.
- Warner, D., Curtin, W., 2009. Origins and implications of temperature-dependent activation energy barriers for dislocation nucleation in face-centered cubic metals. *Acta Materialia* 57 (14), 4267 – 4277.
- Weinberger, C., Cai, W., 2012. Plasticity of metal nanowires. *Journal of Materials Chemistry* 22, 3277–3292.
- Weinberger, C. R., Jennings, A. T., Kang, K., Greer, J. R., 2012. Atomistic simulations and continuum modeling of dislocation nucleation and strength in gold nanowires. *Journal of the Mechanics and Physics of Solids* 60 (1), 84 – 103.
- Woodward, C., Rao, S. I., 2002. Flexible *Ab Initio* boundary conditions: Simulating isolated dislocations in bcc mo and ta. *Phys. Rev. Lett.* 88, 216402.
- Woodward, C., Trinkle, D. R., Hector, L. G., Olmsted, D. L., 2008. Prediction of dislocation cores in aluminum from density functional theory. *Phys. Rev. Lett.* 100, 045507.
- Wu, B., Heidelberg, A., Boland, J. J., 2005. Mechanical properties of ultrahigh-strength gold nanowires. *Nature Materials* 7, 525–529.
- Zhao, M., Slaughter, W. S., Li, M., Mao, S. X., 2003. Material-length-scale-controlled nanoindentation size effects due to strain-gradient plasticity. *Acta Materialia* 51 (15), 4461 – 4469.
- Zheng, H., Cao, A., Weinberger, C. R., Huang, J. Y., Du, K., Wang, J., Ma, Y., Xia, Y., Mao, S. X., 2010. Discrete plasticity in sub-10-nm-sized gold crystals. *Nature Communications* 1, 144.

- Zhou, S. J., Preston, D. L., Lomdahl, P. S., Beazley, D. M., 1998. Large-scale molecular dynamics simulations of dislocation intersection in copper. *Science* 279 (5356), 1525–1527.
- Zhu, T., Li, J., 2010. Ultra-strength materials. *Progress in Materials Science* 55 (7), 710 – 757.
- Zhu, T., Li, J., Samanta, A., Leach, A., Gall, K., 2008. Temperature and strain-rate dependence of surface dislocation nucleation. *Phys. Rev. Lett.* 100, 025502.
- Zuo, L., Ngan, A. H. W., 2006. Molecular dynamics study on compressive yield strength in ni_3al micro-pillars. *Philosophical Magazine Letters* 86 (6), 355–365.
- Zuo, L., Ngan, A. H. W., Zheng, G. P., 2005. Size dependence of incipient dislocation plasticity in ni_3Al . *Phys. Rev. Lett.* 94, 095501.